Supporting Information

Highly Catalytic Activity and Stability of Visible-Light-Driven CO_2 Reduction via $CsPbBr_3$ QDs/Cu-BTC Core-Shell Photocatalysts

Yuanming Hou[1], Yanqing Zhang[1], Shilong Jiao[2,*], Jingyi Qin[1], Luoyu Liu[1], Zhengzheng Xie[1], Zhongjie Guan[1], Jianjun Yang[1], Qiuye Li[1,*], Xianwei Fu[1,*]

[1] Engineering Research Center for Nanomaterials, National & Local Joint Engineering Research Center for Applied Technology of Hybrid Nanomaterials, Henan University, Kaifeng, 475004 Henan, P. R. China

[2] Key Lab for Special Functional Materials of Ministry of Education, Collaborative Innovation Center of Nano Functional Materials and Applications, Henan University, Kaifeng, 475004 Henan, P. R. China

Correspondence and requests for materials should be addressed X. F. (xwfu2021@henu.edu.cn), Q. L (qiuyeli@henu.edu.cn), and sljiao@henu.edu.cn.

1. Chemicals and materials

Lead (II) bromide ($PbBr_2$, 99.0 %) was acquired from MACKLIN (Shanghai Macklin Biochemical Co., Ltd). Cesium carbonate (Cs_2CO_3, 99.9 % metals basis) and trimesic acid were obtained from MACKLIN (Shanghai Macklin Biochemical Co., Ltd). Copper (II) nitrate trihydrate ($Cu(NO_3)_2 \cdot 3H_2O$, AR) and oleic acid (OA) were purchased from Tianjin Kemiou Chemical Reagent Co., Ltd. Ethyl acetate and n-Hexane were purchased from FuYu Chemical Co., Ltd. 1-Octadecene (ODE) was obtained from MACKLIN (Shanghai Macklin Biochemical Technology Co., Ltd). Oleylamine (OAm) was obtained from Aladdin (Shanghai Aladdin Biochemical Technology Co., Ltd.).

2. Materials Characterization

Crystal structures of the synthesized samples were characterized by X-ray diffraction (XRD, X-ray powder diffractometer, D8-ADVANCE German Bruker). Scanning electron microscopy (SEM) images were measured by a Geminisem-500 Zeiss equipment. X-ray photoelectron spectroscopy (XPS) analysis was performed on a PHI-5000C ESCA photoelectron spectrometer with an Al Kα achromatic X-ray source. Transmission electron microscopy (TEM) and energy-dispersive X-ray (EDX) elemental mapping were measured by a TEM-2100 transmitted electron microscope. The photo-absorption properties were detected with a UV-vis spectrometer (UV-2600) in the presence of $BaSO_4$ as the reference. The PL spectra were recorded by a Horiba LabRAM Odyssey with an excitation light source of 325 nm. Photocurrent density curves (i-t curves) and electrochemical impedance spectroscopy (EIS) were investigated on a CHI 600E electrochemical workstation (Shanghai Chenhua) with a three-electrode system, where Pt

foil, Hg/HgO, and fluorine-doped tin oxide (FTO) glass with catalyst films were employed as counter, reference, and the working electrode, respectively. The work electrode was fabricated by the following procedure: 2 mg of the photocatalysts were dispersed into the 1 mL cyclohexane solution to form a homogeneous suspension, which was then dip-dropped on an FTO glass with an exposure area of 1 cm^2. Finally, the film was dried under a vacuum atmosphere at 60 ºC. The acetonitrile containing 0.1 M tetrabutylammonium hexafluorophosphate ($TBAPF_6$) was used as the electrolyte solution, and a 200 W Xe lamp was employed as the light source[1].

3. Photocatalytic CO_2 reduction

Photocatalytic CO_2 reduction was carried out in a sealed quartz reactor.10 mg of the photocatalyst, 28 ml of acetonitrile and 5 μL H_2O were added to the reactor[2]. After sealing, the reactor was purged with high-purity CO_2 before the photocatalytic reaction. Subsequently, a 200 W Xe lamp with a UV-cut filter (420 nm) was used as the visible light source. During the CO_2 photoreduction, the gas products were analyzed by gas chromatography (GC-2018, Shimadzu, Japan) equipped with a flame ionization detector and thermal conductive detector. The H_2 obtained from H_2O splitting was detected by the gas phase chromatograph (GC-2018C, Shimadzu) with the thermal conductivity detector.

The selectivity of products CO is assessed based on the following equation:

$$S_{CO} = \frac{2R_{CO}}{2R_{CO} + 8R_{CH_4}} \times 100\%$$

The total electron consumption rate is calculated as follows:

$$R_e = 2R_{CO} + 8R_{CH_4}$$

Where R_{CO} and R_{CH_4} represent the yield of CO and CH_4. The coefficient in front of R represents the consumed electron number of multi-electron reactions. R_e represents the electron consumption rate.

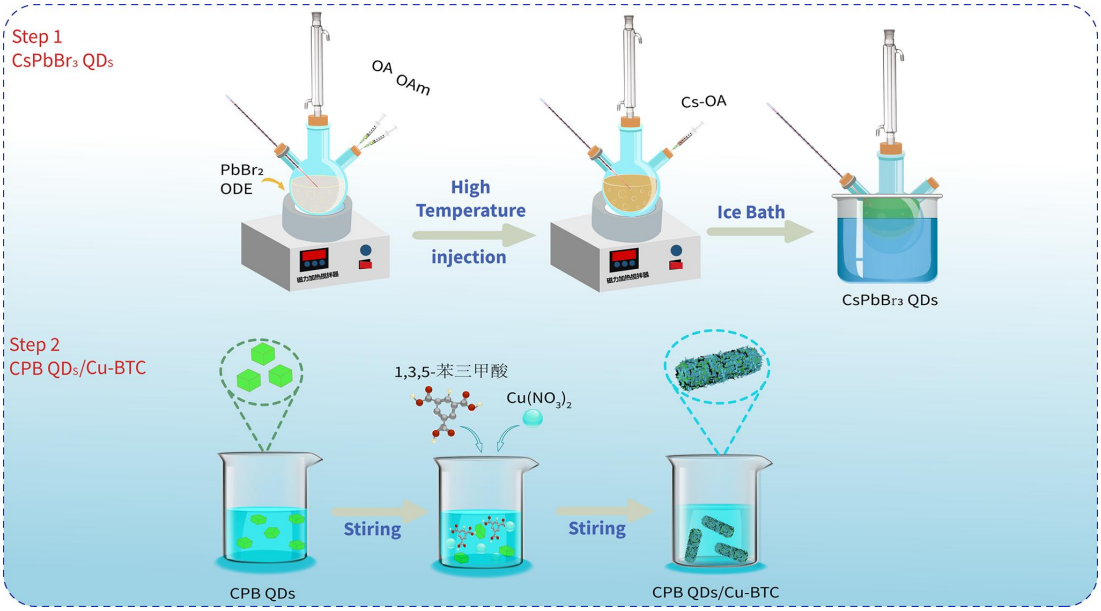

Fig. S1. Schematic diagram of the synthesis of CPB QDs and CPB QDs/Cu-BTC.

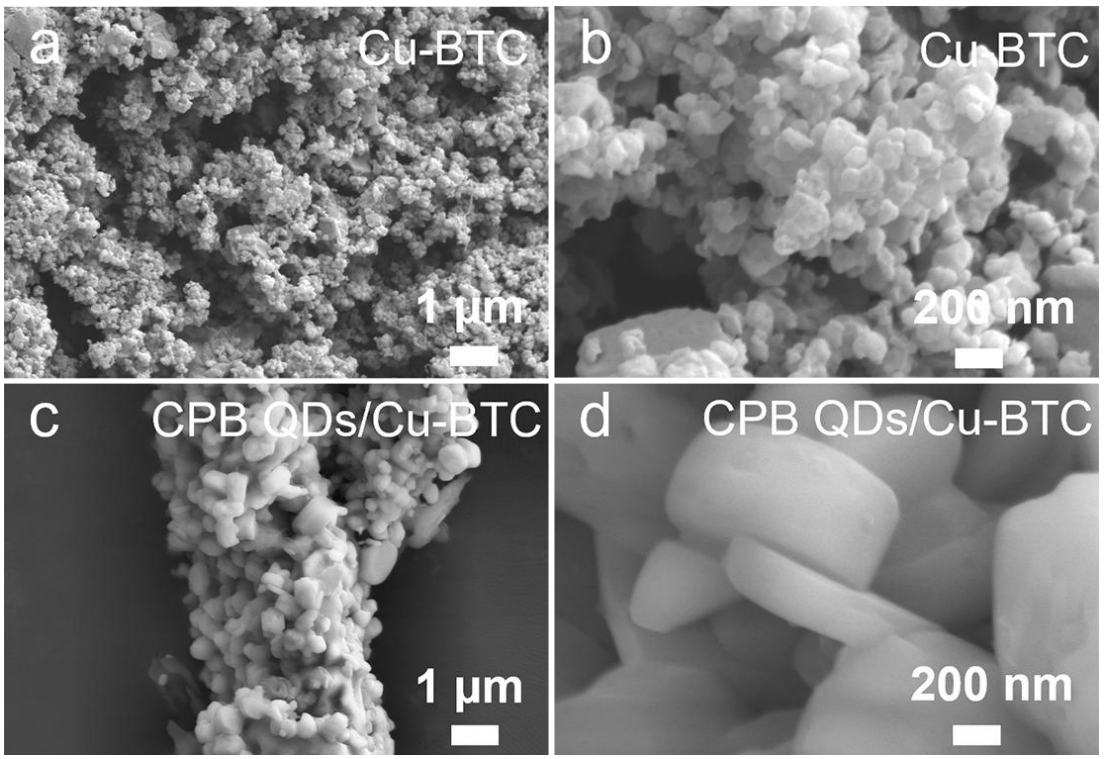

Fig. S2. SEM images of Cu-BTC (a-b) and CPB QDs/Cu-BTC hybrids (c-d).

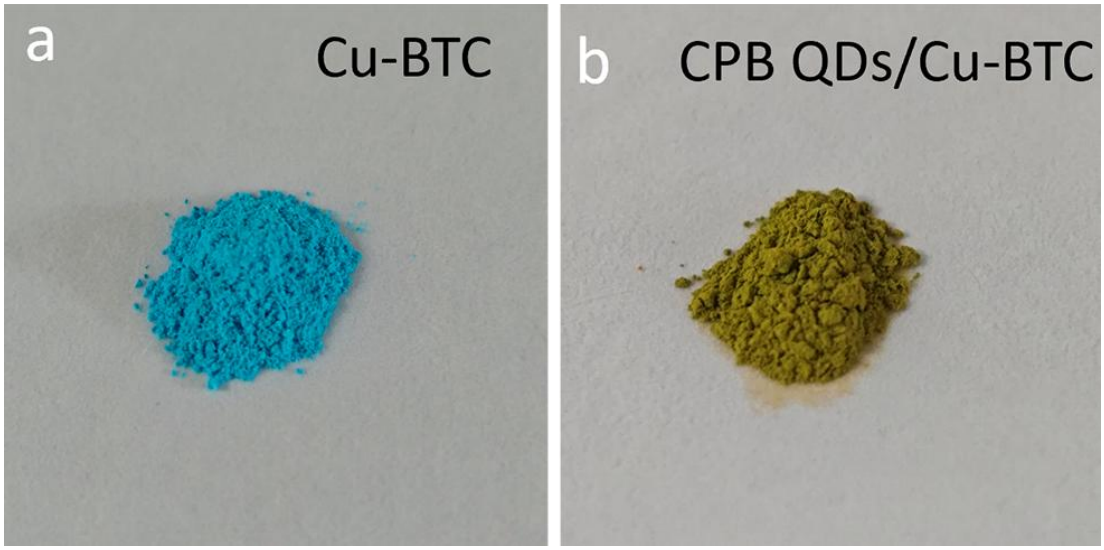

Fig. S3. Photographs of (a) Cu-BTC and (b) CPB QDs/Cu-BTC hybrids.

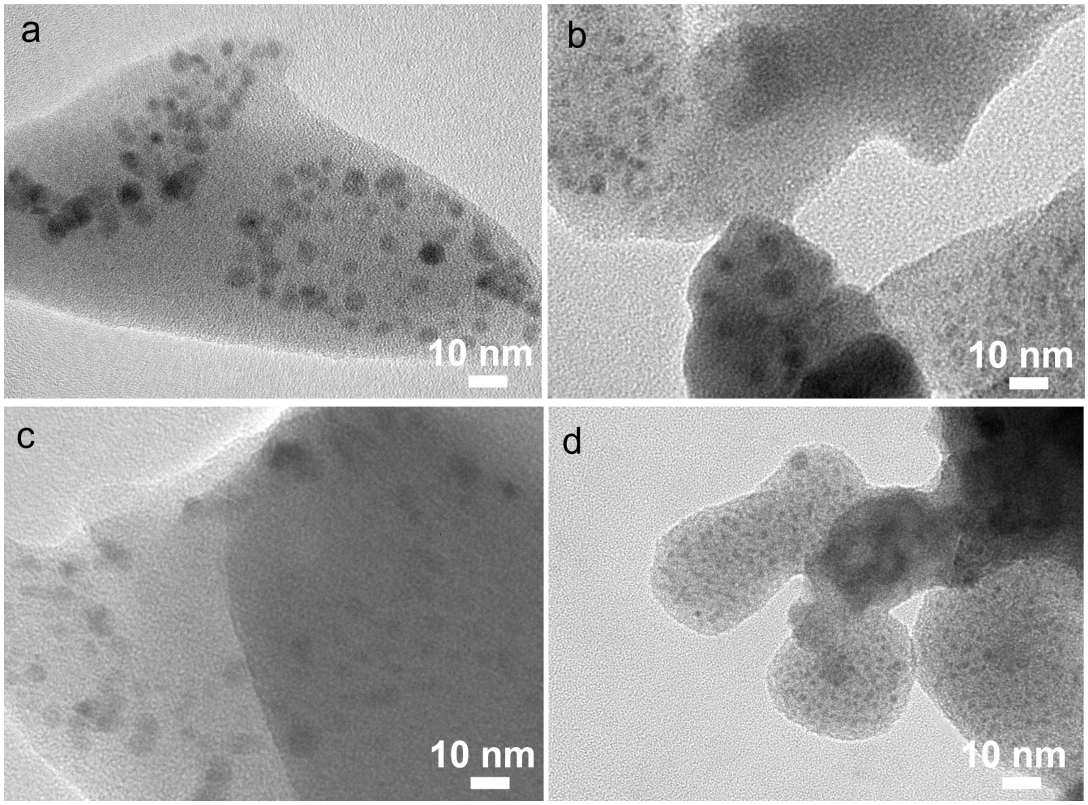

Fig. S4. (a-d) TEM images of the CPB QDs/Cu-BTC composites in different regions.

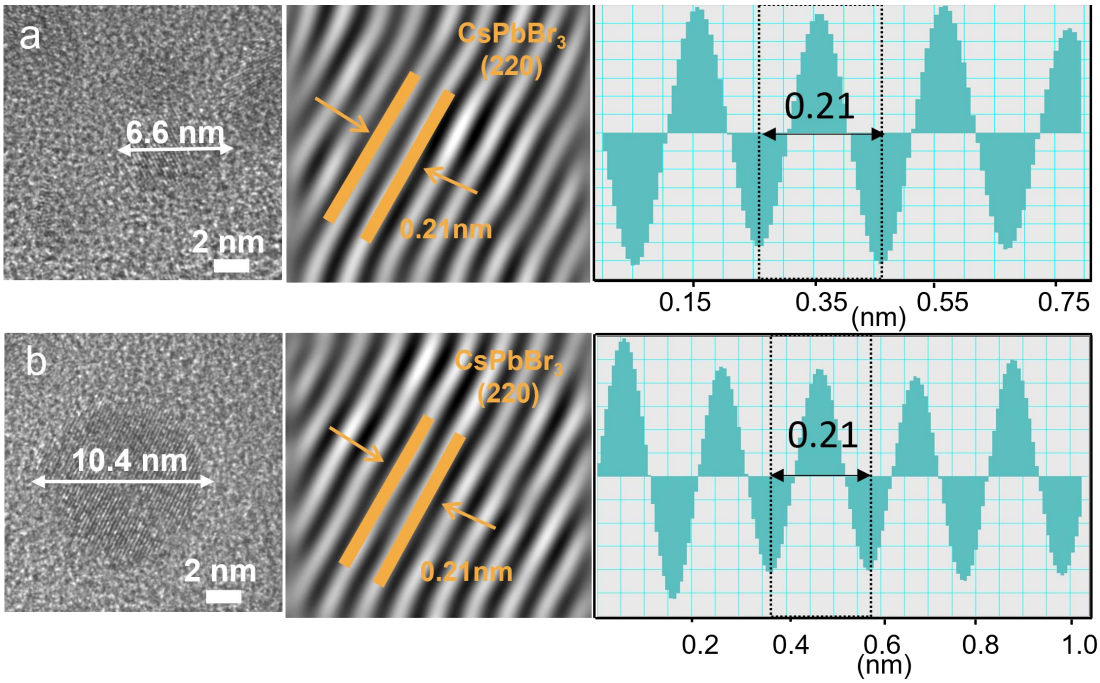

Fig. S5. High-resolution TEM (HRTEM) images of the CPB QDs (a-b).

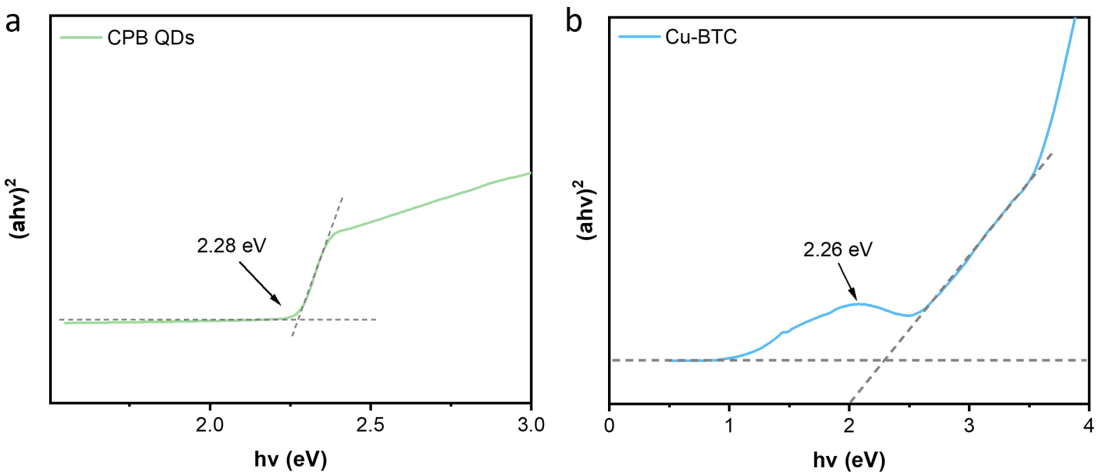

Fig. S6. Tauc plots of CPB QDs (a) and Cu-BTC (b).

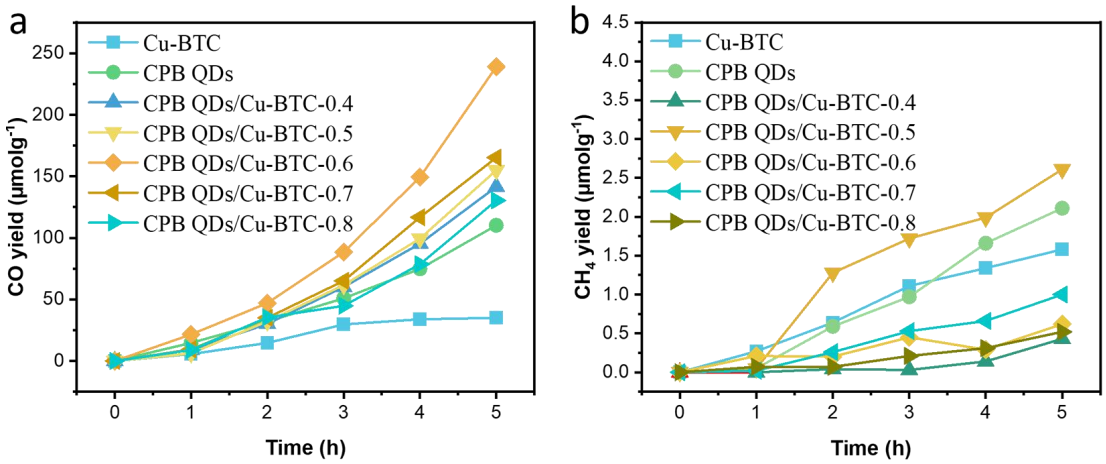

Fig. S7. The time-dependent production rate of CO (a) and CH_4 (b) over various catalysts.

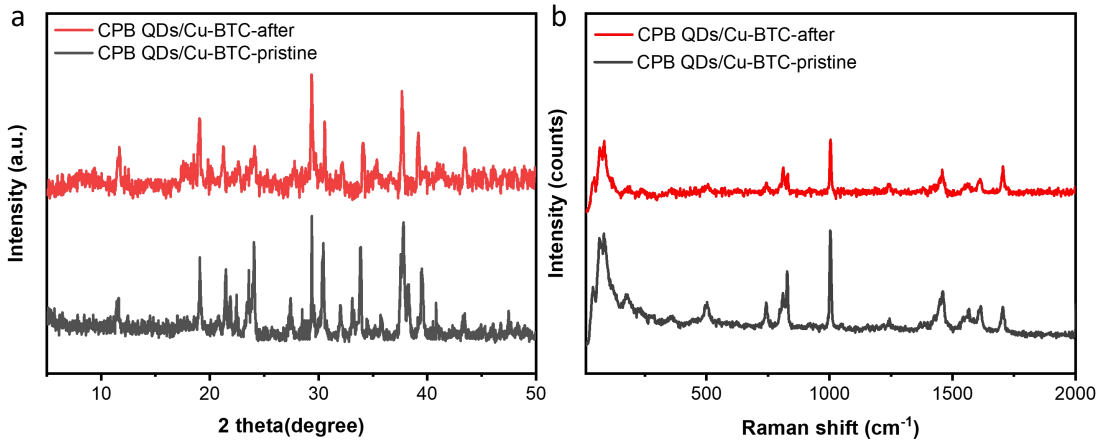

Fig. S8. The XRD (a) and Raman spectra (b) of the CPB QDs/Cu-BTC photocatalyst before and after reaction.

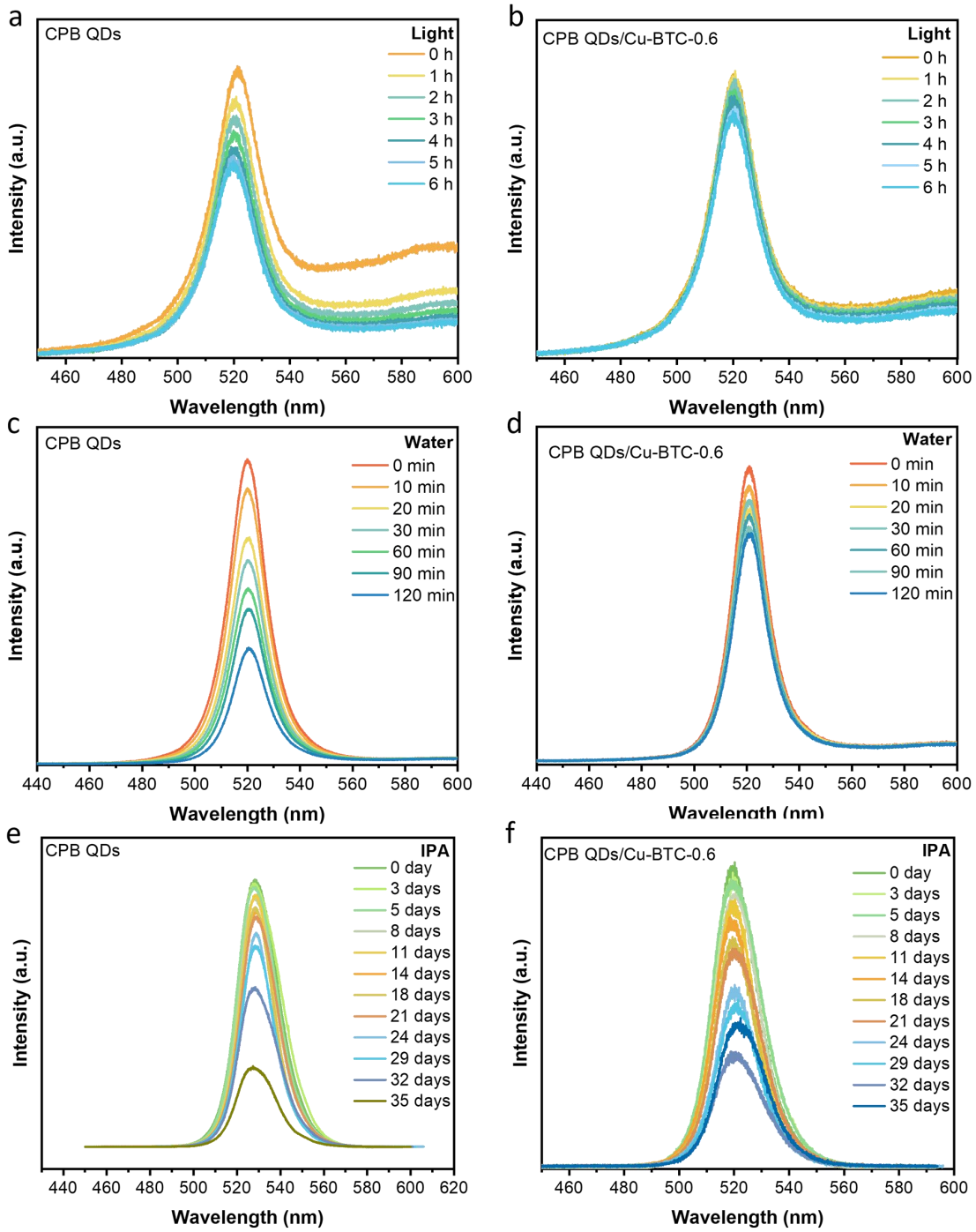

Fig. S9. PL spectra of pure CPB QDs and CPB QDs/ Cu-BTC-0.6 composites under different conditions. (a-b) Under 325 nm laser irradiation for 6 h. (c-d) In water. (e-f) In isopropanol (IPA).

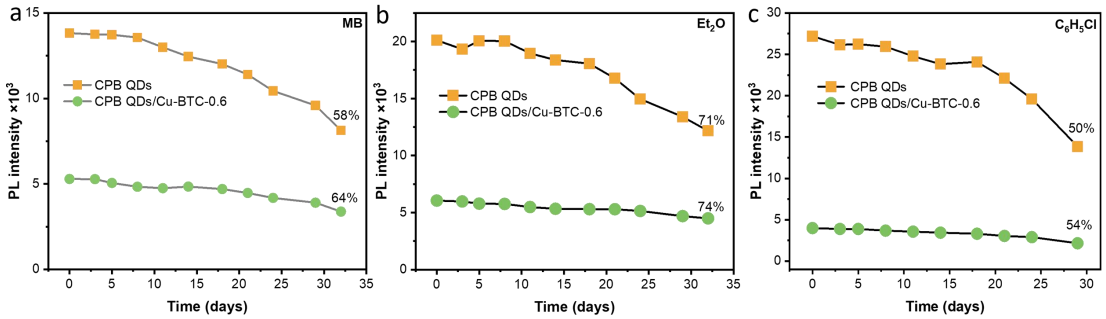

Fig. S10. (a) Time-dependent PL intensity of CPB QDs and CPB QDs/Cu-BTC composites in different solvents. (a) Methylbenzene (MB). (b) Ethyl alcohol (Et_2O). (c) Chlorobenzene (C_6H_5Cl).

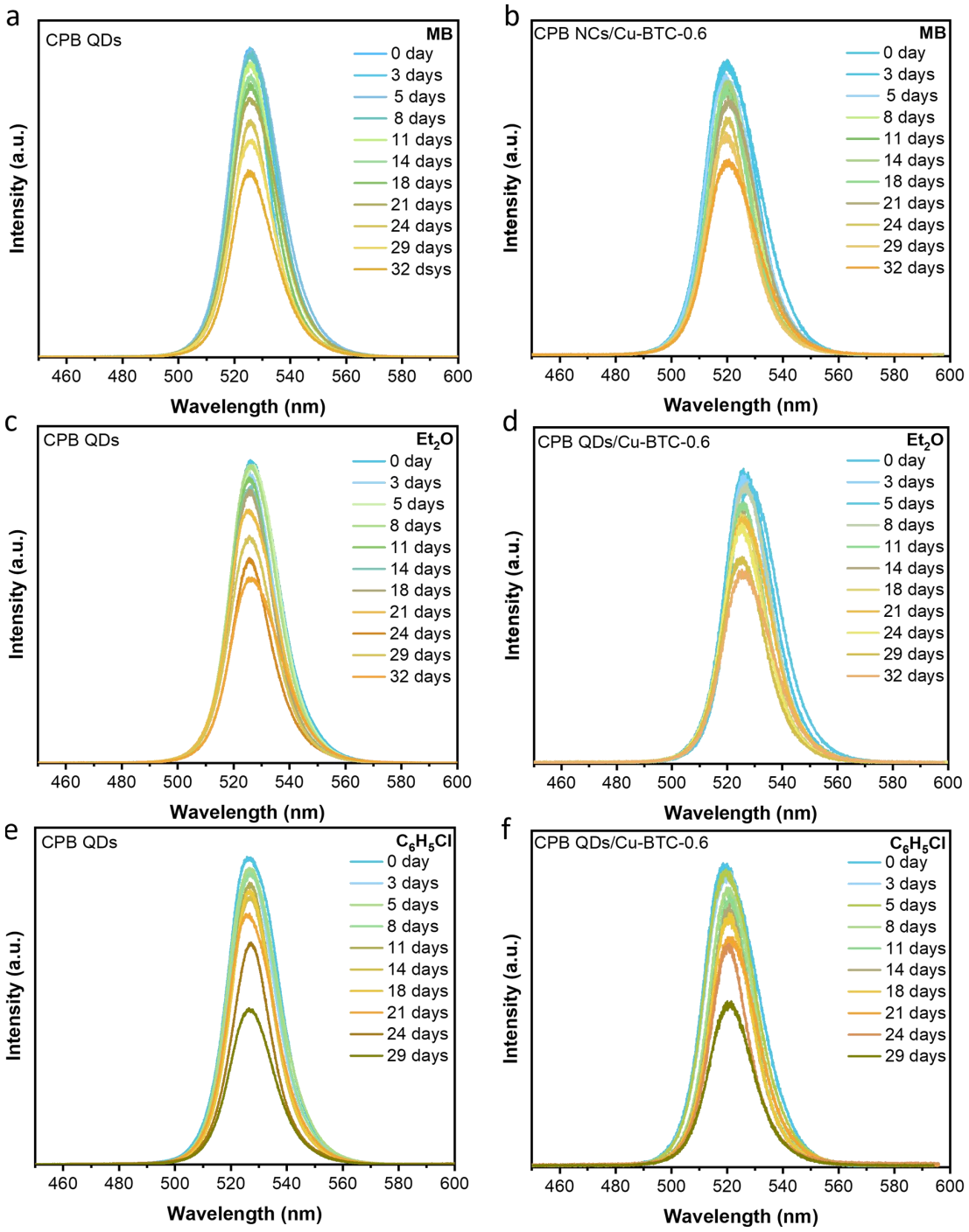

Fig. S11. PL spectra of pure CPB QDs and CPB QDs/Cu-BTC-0.6 composites in methylbenzene (MB) (a-b), ethyl alcohol (Et_2O) (c-d) and chlorobenzene (C_6H_5Cl) (e-f).

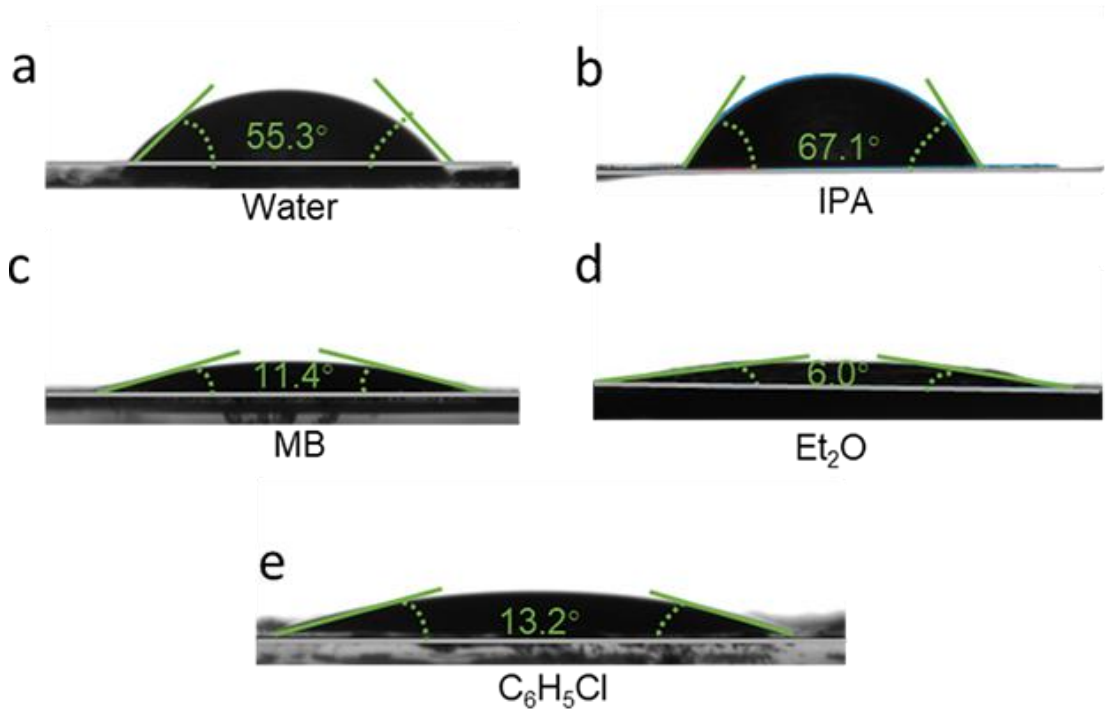

Fig. S12. The images of contact angle between Cu-BTC film and water (a), IPA (b), MB (c), Et_2O (d), C_6H_5Cl (e).

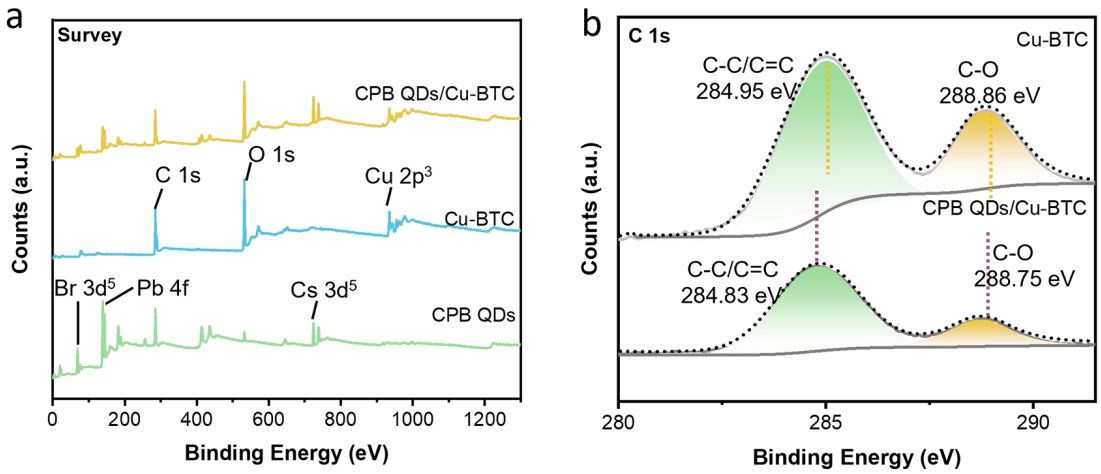

Fig. S13. XPS characterizations of pristine CPB QDs, Cu-BTC, and CPB QDs/Cu-BTC composites. (a) The survey XPS spectra. (b) High-resolution XPS spectra of C 1s.

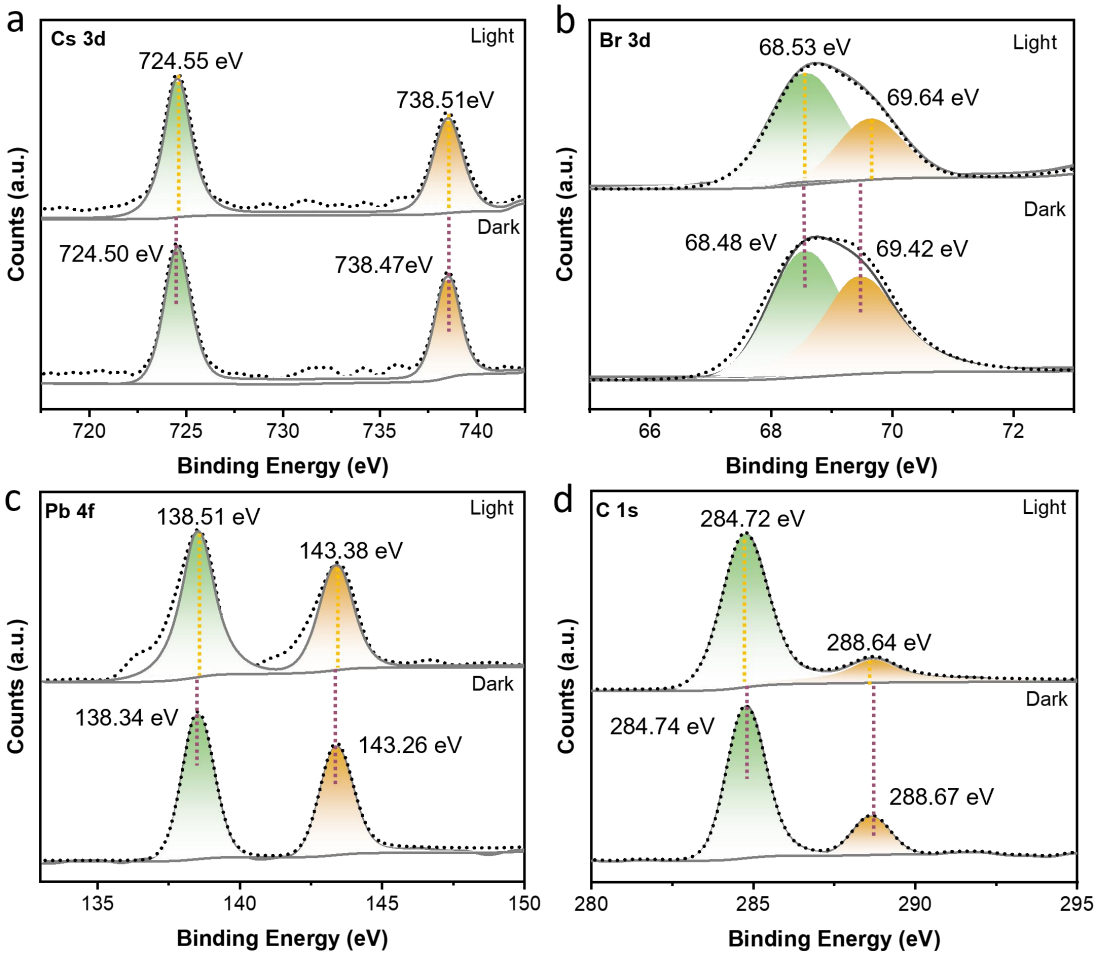

Fig. S14. In-situ XPS characterizations of CPB QDs/Cu-BTC composite in the dark or under visible light irradiation (a-d).

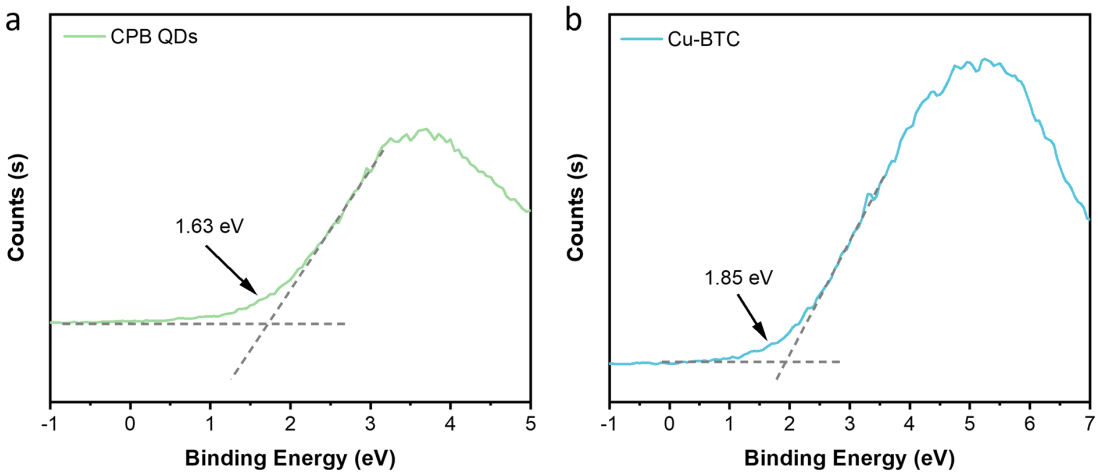

Fig. S15. Valence band spectra of CPB QDs (a) and Cu-BTC (b).

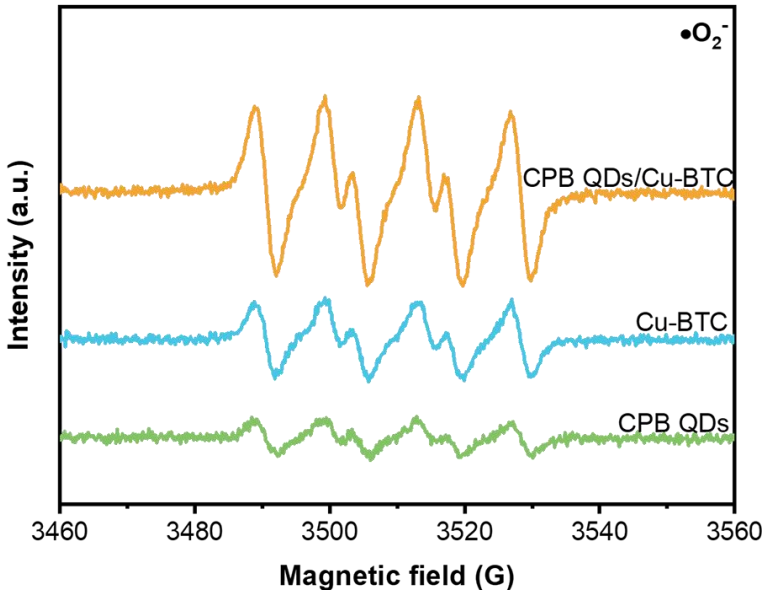

Fig. S16. ESR spectra of $\bullet O_2^-$ trapped by DMPO in the presence of catalysts under visible-light illumination.

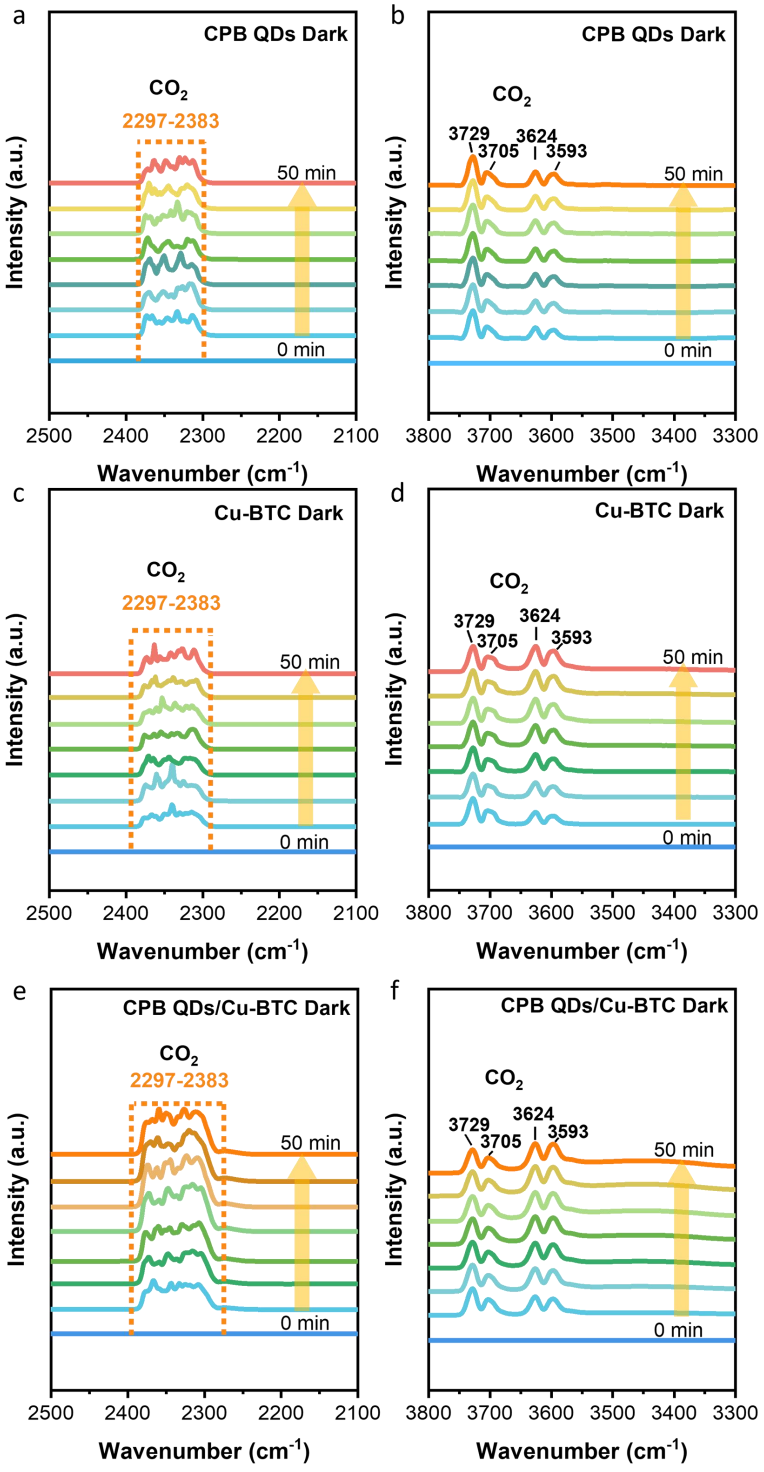

Fig. S17. In-situ DRIFTS spectra for photocatalytic CO_2 reduction over CPB QDs (a-b), Cu-BTC (c-d), and CPB QDs/Cu-BTC (e-f) photocatalysts under dark.

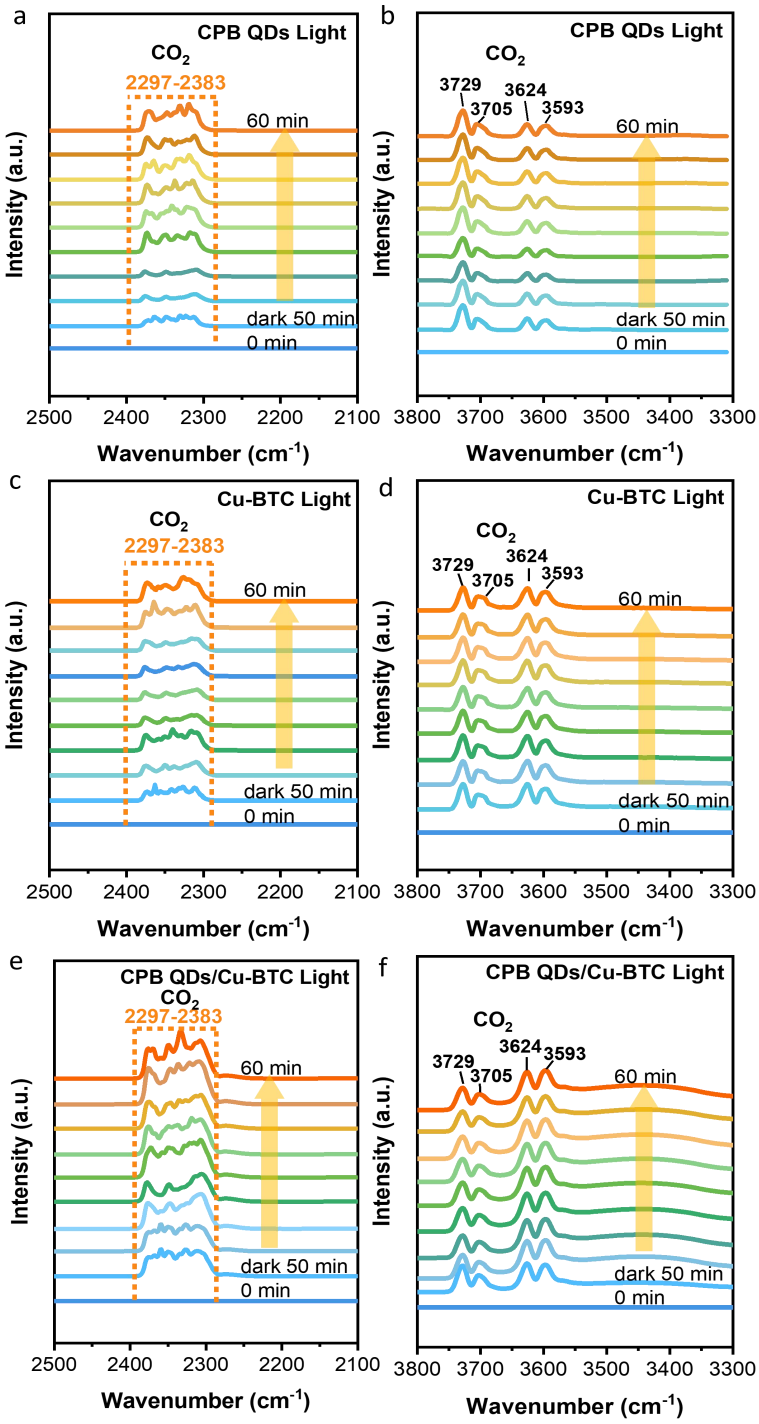

Fig. S18. In-situ DRIFTS spectra for photocatalytic CO_2 reduction over CPB QDs (a-b), Cu-BTC (c-d), and CPB QDs/Cu-BTC (e-f) photocatalysts under simulated solar illumination.

Table S1. Fitting parameters of the TRPL decay traces of CPB QDs and CPB QDs/Cu-BTC-0.6 samples probed at 325 nm.

Sample	τ_1(μ)	A_1	A_1 (%)	τ_2 (μs)	A_2	A_2 (%)	τ_{av}(μ)
CPB QDs	5.31	661.856	16.02	14.58	1118.09	83.98	13.09
CPB QDs/Cu-BTC-0.6	1.44	44.19	44.49	8.42	137.30	55.51	5.31

The two-exponential decay curves were fitted using a non-linear least-squares method with a two-component decay law. The average lifetime (τ_{av}) was then determined using the equation:

$$\tau_{av} = (A_1\tau_1^2 + A_2\tau_2^2)/(A_1\tau_1 + A_2\tau_2)$$

Table S2. Summarize the performance of various visible light-driven photocatalytic CO_2 reduction. EA: ethyl acetate; IPA: isopropanol; ACN: acetonitrile; BA: benzyl alcohol; TEOA: Triethanolamine.

Photocatalysts	Light source	Reaction medium	Yield ($\mu mol\ g^{-1}\ h^{-1}$)	Stability	Ref.
CPB QDs/Cu-BTC	a Xe lamp (λ > 420 nm, 200 mW cm^{-2})	EA/H_2O	CO (47.82)	ten cycles	this work
g-C_3N_4@$Cs_2AgBiBr_6$	a Xe lamp (λ > 420 nm, 80 mW cm^{-2})	TEOA/ EA/H_2O	CO (10.30) CH_4 (0.88)	three cycles	3
$CsPbBr_3$ QD/GO	100 W Xe lamp	H_2O	CO (23.7)	12 h	4
$CsPbBr_3$@ZIF-8	a 100 W Xe lamp (λ > 420 nm,150 mW cm^{-2})	EA	CO (29.630)	six cycles	5
Co2%@$CsPbBr_3$/Cs_4PbBr_6	300 W Xe lamp (λ > 400 nm, 100 mW/cm^2)	H_2O	CO (11.95)	20 h	6
$CsPbBr_3$/Pd	150 W Xe lamp (λ > 400 nm)	H_2O	CO (33.09)	three cycles	7
$CsPbBr_3$ QDs/UiO-66(NH_2)	300 W Xe lamp (λ>420 nm)	EA/ H_2O	CO (8.21) CH_4 (0.26)	three cycles	8
$CsPbIxBr_{3-x}$ PQDs/PES	300 W Xe lamp (AM 1.5G)	H_2O	CO (32.45)	2 h	9
$CsPbBr_3$/PCN	300 W Xe lamp	ACN/ H_2O	CO (148.9)	three	10

	(λ>420 nm)			cycles	
$In_4SnS_8/Cs_3Bi_2Br_9$	300 W argon lamp (λ>420 nm)	H_2O	CO (9.55)	three cycles	[11]
MCM41@ 50wt% CBB	300 W Xe lamp (λ > 420 nm)	H_2O	CO (17.27)	eight cycles	[12]

References

1 L. Ren, Y. Wang, M. Wang, S. Wang, Y. Zhao, C. Cazorla, C. Chen, T. Wu and K. Jin, *J. Phys. Chem. Lett.*, 2020, **11**, 2577–2584.

2 Y. Zhang, W. Chen, M. Zhou, G. Miao and Y. Liu, *ACS Appl. Energy Mater.*, 2021, **4**, 9154–9165.

3 W. Xiong, Y. Dong and A. Pan, *Nanoscale*, 2023, **15**, 15619.

4 Y.-F. Xu, M.-Z. Yang, B.-X. Chen, X.-D. Wang, H.-Y. Chen, D.-B. Kuang and C.-Y. Su, *J. Am. Chem. Soc.,* 2018, **1**, 5083–5089.

5 Z.-C. Kong, J.-F. Liao, Y.-J. Dong, Y.-F. Xu, H.-Y. Chen, D.-B. Kuang and C.-Y. Su, *ACS Energy Letters*., 2018, **3**, 2656−2662.

6 Y.-F. Mu, W. Zhang, X.-X. Guo, G.-X. Dong, M. Zhang and T.-B. Lu, *ChemSusChem*, 2019, 4769–477.

7 Y.-F. Xu, M.-Z. Yang, H.-Y. Chen, J.-F. Liao, X.-D. Wang and D.-B. Kuang, *ACS Appl. Energy Mater.*, 2018, **1**, 5083–5089.

8 S. Wan, M. Ou, Q. Zhong and X. Wang, *Chem. Eng. J*, 2019, **358**, 1287–1295.

9 Y. Jiang, J.-F. Liao, H.-Y. Chen, H.-H. Zhang, J.-Y. Li, X.-D. Wang and D.-B. Kuang, *Chem*, 2020, **6**, 766–780.

10 M. Ou, W. Tu, S. Yin, W. Xing, S. Wu, H. Wang, S. Wan, Q. Zhong and R. Xu, *Angew. Chem. Int. Ed.*, 2018, **57**, 13570–13574.

11 Z. Zhang, M. Wang, Z. Chi, W. Li, H. Yu, N. Yang and H. Yu, *Appl. Catal B: Environ*, 2022, **313**, 121426.

12 Z. Cui, P. Wang, Y. Wu, X. Liu, G. Chen, P. Gao, Q. Zhang, Z. Wang, Z. Zheng, H. Cheng, Y. Liu, Y. Dai and B. Huang, *Appl. Catal B: Environ*, 2022, **310**, 121375.